RESEARCH ARTICLE
SPACE PHYSICS

Earth and Planetary Physics
9: 1157–1162, 2025
doi: 10.26464/epp2025073

Moonward deviation of the solar wind

Chao Wei[1,2], Hui Zhang[1,2,3*], QuanMing Lu[4], JunYi Ren[4], XiaoWei Ma[1,2], and RunZe Li[1,2]

[1]Key Laboratory of Planetary Science and Frontier Technology, Institute of Geology and Geophysics, Chinese Academy of Sciences, Beijing 100029, China;
[2]College of Earth and Planetary Sciences, University of Chinese Academy of Sciences, Beijing 100049, China;
[3]Heilongjiang Mohe National Observatory of Geophysics, Institute of Geology and Geophysics, Chinese Academy of Sciences, Beijing 100029, China;
[4]CAS Key Laboratory of Geospace Environment, Department of Geophysics and Planetary Science, University of Science and Technology of China, Hefei 230026, China

Key Points:

- Unexpected, large-scale moonward deviations are found in the solar wind upstream of the Moon.
- The longer the duration of the interaction, the greater the moonward deviations.
- The Moon's influence on the solar wind extends beyond mere absorption and reflection.

Citation: Wei, C., Zhang, H., Lu, Q. M., Ren, J. Y., Ma, X. W., and Li, R. Z. (2025). Moonward deviation of the solar wind. *Earth Planet. Phys.*, *9*(6), 1157–1162. http://doi.org/10.26464/epp2025073

Abstract: The solar wind's interaction with the Moon has traditionally been understood through the Moon's absorption of solar wind particles and the formation of a plasma cavity on its nightside, known as the lunar wake. This study reveals unexpected, large-scale perturbations in the solar wind upstream of the Moon, using 11 years of data from the OMNI and ARTEMIS (Acceleration, Reconnection, Turbulence and Electrodynamics of Moon's Interaction with the Sun) missions (2012–2023). We find systematic moonward deviations of ~tens of km/s in a direction perpendicular to the solar wind (moonward), at altitudes of up to 1000 km, particularly when the interplanetary magnetic field (IMF) lines are oblique to the solar wind (30° < θ < 60°) and connected to the lunar dayside. The longer the duration of the interaction, the greater the moonward deviation. These perturbations can be explained by neither solar wind pickup of the reflected ions, nor lunar wake dynamics. Instead, they appear to correlate with magnetic connectivity between the ARTEMIS probes and the lunar surface, suggesting a more complex solar wind interaction than previously thought.

Keywords: plasma-moon interaction; moonward deviation; IMF connectivity; lunar upstream perturbations

1. Introduction

When the Moon is immersed in the solar wind, the flow of solar wind plasma in the lunar wake can undergo large-scale perturbations. The interplanetary magnetic fields (IMFs) are able to pass through the Moon unaltered (Lyon et al., 1967), while the supersonic solar wind plasmas impact onto the lunar surface and are absorbed. This creates a cylindrical plasma cavity behind the Moon, known as the lunar wake (Sonett, 1982). There are two primary ways by which the solar wind can enter the wake: either perpendicular to the magnetic field lines or parallel to them. Due to the plasma pressure gradient at the boundary of the lunar wake (Ness et al., 1968), the ambient plasma can be sucked into the cavity across the magnetic fields, causing magnetic field compression in the central wake and magnetic field depletion on the wake boundary (Whang and Ness, 1970). The ambipolar electric field, which has been confirmed by observations from the Wind satellite beyond 6.5 lunar radii, can also accelerate solar wind ions into the cavity along the magnetic field lines (Halekas et al., 2005a; Zhang H et al., 2014). When the magnetic field lines are oblique to the background solar wind, the field-aligned acceleration of ions can increase the plasma bulk velocity on one side of the wake, while decrease it on the other side (Ogilvie and Ness, 1969; Clack et al., 2004).

In the region outside of the lunar wake, the plasma is generally understood to remain unperturbed. On the dayside of the Moon, the lunar surface typically exhibits an electric potential ranging from −10 to 18 volts; whether the potential is positive or negative is primarily determined by the dynamic between the photoemission effect and plasma thermal effect (Freeman and Ibrahim, 1975). The electric fields generated by the surface charge are confined within a thin plasma layer known as the Debye sheath, which extends approximately 10 meters above the lunar surface. Therefore, large-scale perturbations of the solar wind velocity by the dayside electric fields are unexpected in the vast space over the dayside surface. Previous studies have shown that some solar wind particles can be reflected from the lunar surface, or from crustal magnetic fields into the near-lunar space, where they can be picked up by the background solar wind, making perturbations in the magnetic fields and solar wind. However, these reflected

First author: C. Wei, chaowei@mail.iggcas.ac.cn
Correspondence to: H. Zhang, hzhang@mail.iggcas.ac.cn
Received 28 MAR 2025; Accepted 28 APR 2025.
First Published online 27 JUN 2025.

ions are limited to altitudes of approximately 400 kilometers, and the perturbations beyond this range cannot be attributed to the pickup process (Zhang TX et al., 2020). Nevertheless, when the background plasma conditions change, for example, the Moon enters the Earth's magnetosphere and the ambient plasma temperature increases, intense negative potentials (−500 V) are unexpectedly measured over the dayside surface by the Electron Reflectometer instrument onboard Lunar Prospector. These potentials are thought to arise from the extremely strong plasma thermal effect that overwhelms the photoemission effect (Halekas et al., 2005b, 2011; Poppe et al., 2011). Simulation studies also indicate that a majority of photoelectrons are electrically trapped within altitudes roughly several hundred meters above the dayside surface (Poppe et al., 2011). The influences of these large-scale electric fields on the solar wind velocities remain poorly understood and require further investigation.

In our study, data from the OMNI and ARTEMIS missions reveal that the solar wind bulk velocity has been noticeably influenced at the upstream region of the Moon's dayside, particularly when the IMFs connect to the dayside of the Moon. These perturbations manifest as systematic moonward deviations of the solar wind flow in the plane determined by the solar wind velocity and the IMF, at altitudes of up to 1000 km. The longer the duration of interaction between a magnetic field line and the Moon, the greater the magnitude of the moonward deflection. This suggests that the Moon's interaction with the solar wind may involve more than simple absorption and reflection. This phenomenon provides new insights into the Moon's interaction with solar wind.

2. Data and Coordinates

OMNI data are solar wind observations that have been measured elsewhere, such as the L1 Lagrange point, then time-shifted to the nose of the Earth's bow shock, as an indicator of the upstream solar wind conditions for the Earth. They provide upstream solar wind parameters, including IMFs and solar wind velocities. The OMNI data are obtained from NASA/Goddard Space Flight Center's (GSFC) OMNI website. The time resolution of the data is 1min and 5 min. In our study, we adopt the 1 min resolution data.

The ARTEMIS mission, the extension of the THEMIS mission, consists of two identical satellites, probes P1 and P2 (Angelopoulos, 2011). The perigees of the two satellites are approximately 100 km, and the apogees are approximately 19,000 km (Angelopoulos, 2011). We use the magnetic field observations from the fluxgate magnetometer (FGM) instrument (Auster et al., 2008) and the ion velocity observations from electrostatic analyzer (ESA) instrument (McFadden et al., 2008) onboard the ARTEMIS at a time resolution of 3 s. In order to test the influence of the Moon on the upstream solar wind velocity, our database includes data collected while the Moon is immersed in the solar wind, and ARTEMIS satellites are not simultaneously in the lunar wake.

We use the data from OMNI in the coordinate system of Geocentric Solar Ecliptic (GSE) and the data from ARTEMIS in the coordinate system of Selenocentric Solar Ecliptic (SSE), respectively. SSE is thought to be approximately identical to GSE, considering that the Earth–Moon distance is nearly negligible compared to the Earth–Sun distance. To relate observations to the directions of the IMF and solar wind velocity, a new orthogonal coordinate system is introduced in our study, which we refer to as the lunar solar magnetic system (LSM) as shown in Figure 1. The LSM coordinate system is related to the direction of the IMF. The direction of the X axis of LSM is identical to the $+X$ direction of SSE. If the cone angle (CA) between the IMF and $+X$ is larger than 90 degrees, Z is taken along the direction of $\boldsymbol{X} \times \boldsymbol{B}_{\mathrm{IMF}}$; If the cone angle between the IMF and $+X$ is smaller than 90 degrees, Z is taken along the direction of $-\boldsymbol{X} \times \boldsymbol{B}_{\mathrm{IMF}}$; Y completes the orthogonal set through $\boldsymbol{Z} \times \boldsymbol{X}$. In this way, the IMFs remain parallel to the XY plane and always satisfy $B_x B_y < 0$. In the LSM coordinate system, the moon is located at the center, and the velocity direction of the background solar wind is mainly in the X direction. If the satellite is on the $-Y$ side and a flow deflection in the $+Y$ direction occurs, it is considered a moonward deviation. Similarly, if the satellite is on the $+Y$ side and a flow deflection in the $-Y$ direction occurs, it is considered a moonward deviation.

3. Observations

We conducted a statistical study based on 11 years of data, from January 1, 2012, to January 1, 2023. Figure2a involves all the solar wind velocity observations from OMNI, while Figure 2b involves the solar wind ion velocity observations from ARTEMIS, when the Moon is in the solar wind and ARTEMIS probes are not simultaneously within the lunar wake. Geocentric elongation of the Moon relative to the Sun is limited to a maximum of 120 degrees, ensuring that the Moon is immersed in the solar wind. Additionally, in the SSE coordinate system, the criteria $x > 0$ or $x < 0$ and $\sqrt{y^2 + z^2} > (R_L + 0.1 \times |x|)$ guarantees that the ARTEMIS probes are outside the lunar wake (R_L = 1738 km). The probability density distribution of the two components of undisturbed solar wind velocity, V_y and V_z in GSE, is shown in Figure 2a. In this YZ-plane of GSE, the probability density distribution is roughly centrally symmetric around the origin. ARTEMIS probes experience the motion of the Moon around the Sun at a velocity of 29.8 km/s, and the data have not been measured in a stellar inertial reference

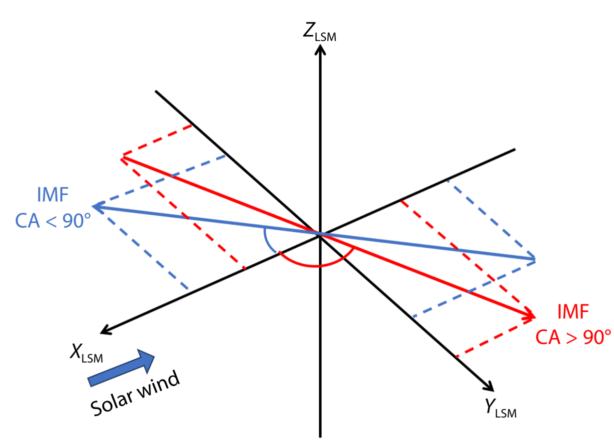

Figure 1. The orthogonal coordinate system used in this paper, referred to as the lunar solar magnetic system (LSM). The origin of the system is set at the center of the Moon. The direction of the X axis of LSM is identical to the $+X$ direction of the Selenocentric Solar Ecliptic (SSE).

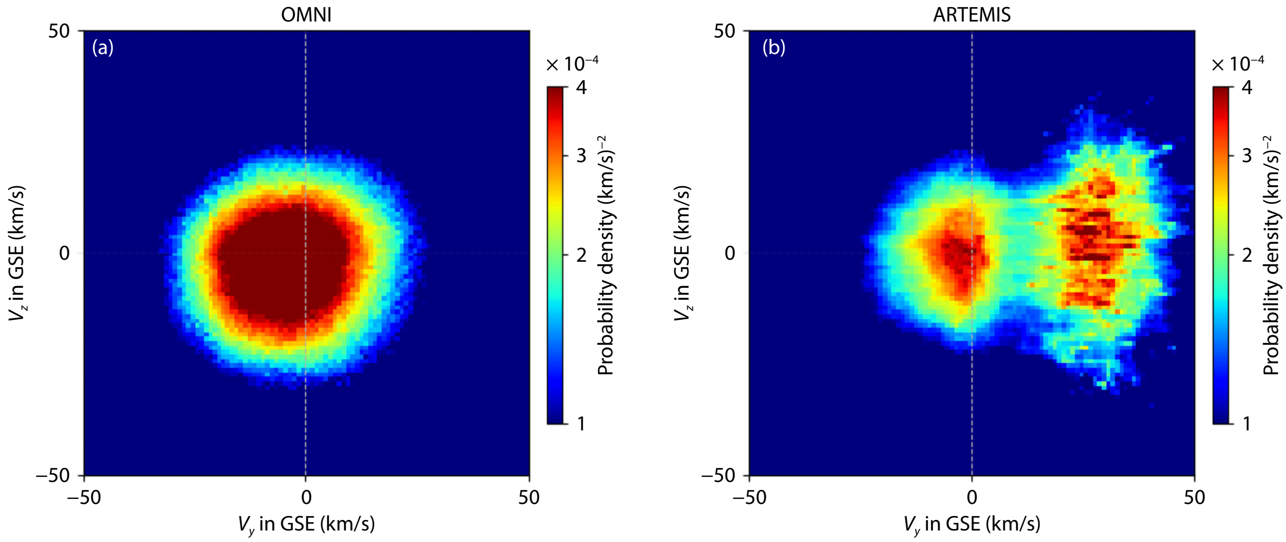

Figure 2. Probability density distributions of solar wind velocity perturbations in the *YZ* plane observed from OMNI (a) and ARTEMIS (b). The bin size is 1 km/s × 1 km/s.

frame. To eliminate this orbit effect around the Sun, the ion velocity vectors observed by ARTEMIS in the *Y* direction of SSE are subtracted by 29.8 km/s. The distribution of the two components, V_y and V_z, in the *YZ* plane of SSE (GSE) following this recalibration is shown in Figure 2b. There are two patterns clearly shown in this distribution, and a majority of data points cluster near the origin which is understood to be the undisturbed solar wind, whereas the others shift in the +*Y* direction by several tens of km/s, which is unexpected.

The IMF conditions corresponding to the data points of ARTEMIS in Figure 2b are particularly selected in particular from the OMNI dataset. Figure 3 depicts the probability density distribution of the IMF clock angles, which are defined as the deviation angles of IMFs from the +*Z* direction within the *YZ* plane of GSE, showing that the IMF clock angles are concentrated near 90 and 270 degrees, respectively. This indicates that the IMFs are nearly parallel to the ecliptic plane.

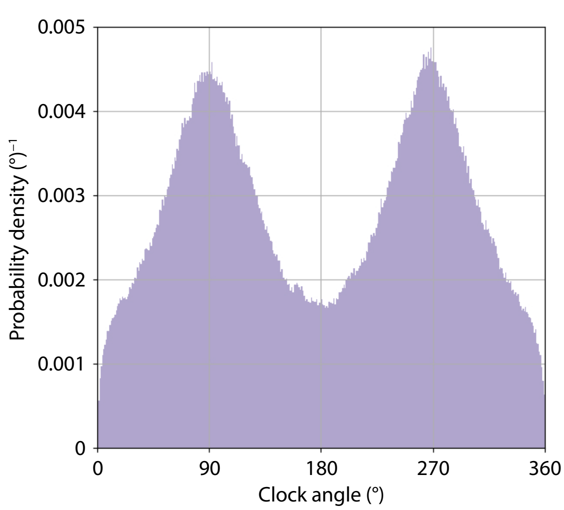

Figure 3. The IMF conditions from OMNI. The probabilities are plotted as a function of the IMF clock angles, which range from 0 to 360 degrees.

To facilitate the study of the relationship between these flow deviations in Figure 2b and the directions of the IMFs, we have transformed all the data, including the satellite positions, plasma flow vectors, and magnetic fields, from the SSE into the LSM coordinate system, in which the IMFs are purely parallel to the *XY* plane pointing toward either the second or the fourth quadrants. After the coordinate system transformations, the solar wind velocities observed by OMNI still exhibit a centrosymmetric distribution, slightly elongated in the ±*Y* directions, as depicted in Figure 4a. For the ARTEMIS data points in Figure 2b at which the ARTEMIS probes have never been magnetically connected to the surface of the Moon, the V_Y and V_Z velocity perturbations in the LSM coordinate system (Figure 4b) show a similar pattern to that of the undisturbed solar wind (Figure 4a). The velocity perturbations observed by ARTEMIS satellites when they are magnetically connected to the dayside lunar surface are shown in Figure 4c. This velocity perturbation distribution becomes obviously asymmetric, showing an overall deviation by several tens of km/s in the +*Y* direction, as well as some data points with deviation in the −*Y* direction. By comparing Figures 4b and 4c, it is concluded that the magnetic connectivity of ARTEMIS to the lunar surface appears critical to the flow deviations. In other words, the group of data points shifted by tens of km/s in Figure 2b are situated on those IMF field lines that have been connecting to the Moon.

We then primarily observe the large-scale deviations of solar wind flow, especially when the ARTEMIS probe, P1 or P2, is magnetically connected to the surface of the Moon (Figure 4c). According to the geometry of the IMFs that are nearly parallel to the solar ecliptic plane, coupled with the fact that ARTEMIS is an equatorial satellite, when the satellite is magnetically connected to the dayside of the Moon, the position coordinates of ARTEMIS corresponding to all the datapoints in Figure 4c are primarily with $X > 0$ and $Y < 0$ and only occasionally with $X > 0$ and $Y > 0$ in the SSE coordinate system (Figure 5a), where the moonward flow deviations interpret why the +*Y* flow perturbations, instead of −*Y*, dominate in Figure

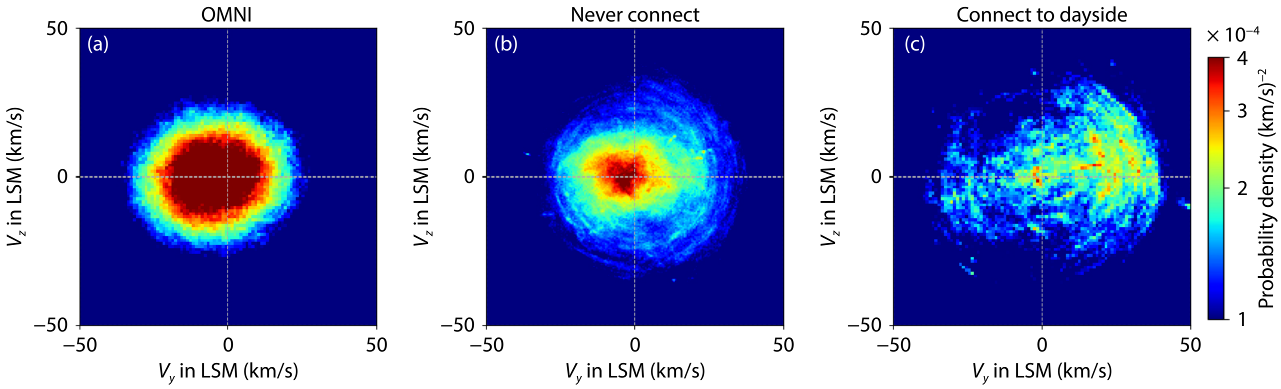

Figure 4. Probability density distributions of solar wind velocities in the *YZ* plane of LSM coordinate system observed from OMNI (a) and ARTEMIS (b, c). (a) involves observations from OMNI in which the ARTEMIS probes never magnetically connect to the lunar surface; (b) involves parts of the data in Figure 2b of ARTEMIS, when the two probes have never magnetically connected to the Moon; (c) involves parts of the data in Figure 2b of ARTEMIS when the probe, P1 or P2, is magnetically connecting to the dayside of the Moon. The bin size is also 1 km/s × 1 km/s.

2b. This distribution also indicates that the IMFs corresponding to the datapoints adopted here are mainly configured according to the Parker spiral structure. After transforming these satellite positions into the LSM coordinate system, the IMFs are now purely parallel to the *XY* plane, and always satisfying $B_xB_y < 0$, the datapoints are now mainly located in the quadrants with $X > 0$ and $Y < 0$ and sometimes with $X < 0$ and $Y > 0$, as shown in Figure 5b. The red and green colors in the Figure 5b indicate that the regions in which the flow perturbations have been frequently detected extend up to about 1000 km from the lunar surface. We select the bins of Figure 5b with the probability density greater than 0.2, to investigate the median values of V_y. As illustrated in Figure 5c, the red color represents the velocity deviation in the +*Y* direction, or as we described it, the moonward flow deflection. In particular, the dependence of the flow deviation on the acute intersection angle θ between the IMF and *X* axis of LSM is investigated. When $30° < \theta < 60°$, the IMFs pass through the Moon obliquely, with the magnetic field lines either pointing toward or away from the Sun. The spatial distributions of the ARTEMIS probes in the SSE coordinate system are shown in Figure 5d. After transforming the coordinate system into the LSM system, their distributions are illustrated in Figure 5e. Similarly, if the probability density in a bin in Figure 5e exceed 0.2, the median values of V_y are calculated and plotted in Figure 5f. Under the condition of oblique IMFs, the V_y distribution displays an obvious moonward deflection. Additionally, as the magnetic field lines propagate further downstream—that is, as their interaction time with the Moon increases—the magnitude of the deviation also increases (the V_y perturbations in the downstream region are greater than those in the upstream region, as seen in Figure 5f). As a supplement, we point out that when the intersection angle θ is too small (<30°) or too large (>60°), the velocity perturbation in the spatial distribution, either positive or negative, no longer demonstrates a clear pattern (not shown).

4. Discussion

Our study reveals significant perturbations in the solar wind velocity near the Moon, particularly when the IMF lines are connected to the dayside lunar surface. These perturbations manifest as a systematic deviation of the solar wind flow towards the Moon, as illustrated in Figures 2b, 4c, 5c and 5f. This phenomenon cannot be fully explained by the current theories of solar wind interaction with the Moon, which traditionally focus on ion reflection and absorption, and lunar wake formation.

The observed large-scale perturbations in the solar wind velocity cannot be attributed to the pickup of ions reflected from the Moon. When the reflected ions move backward into the upstream solar wind, they can be picked-up by the incident solar wind and cause perturbations in both magnetic fields and solar wind velocity. These perturbations, however, are limited to altitudes of 400 km (Fatemi et al., 2014; Zhang TX et al., 2020), because the reflected ions, which gyrate at a velocity comparable to the bulk velocity of the solar wind (~ 400 km/s), can only reach those altitudes. In our study, the flow perturbations detected by the ARTEMIS probes are located at altitudes of up to 1000 km above the lunar surface, as shown in Figures 5a, 5b, 5d, and 5e, far beyond the range of the reflected ions. Therefore, ion reflection is unlikely to be the driver of these perturbations.

The entry of ambient solar wind plasma into the cavity, driven by either pressure gradients or ambipolar electric fields, surely create velocity perturbations in the lunar wake (Ness et al., 1968; Halekas et al., 2005a; Zhang H et al., 2014). Recent studies have demonstrated that protons, reflected on the dayside lunar surface and entering the lunar wake due to their large gyroradii, can also disturb the flow inside the wake by introducing positive potential structures (Xu SS et al., 2020). All these flow perturbations are confined within the lunar wake. Our observations, however, are focused in the upstream solar wind, which is traditionally considered unperturbed.

The large-scale perturbations in the solar wind velocity show the potential drop around the moon. The 2D PIC simulation potential by Nakagawa and Kimura shows that the solar wind electronic absorptions by the lunar surface lead to the potential drop around the Moon (Nakagawa and Kimura, 2011), with a magnitude comparable to the electron kinetic energy. Moreover, the potential drop is controlled by the direction of IMF, and may be found upstream from the Moon in places where the IMF is connected to the lunar body. These features are basically consistent with the observations shown in this paper. The main problem is that the

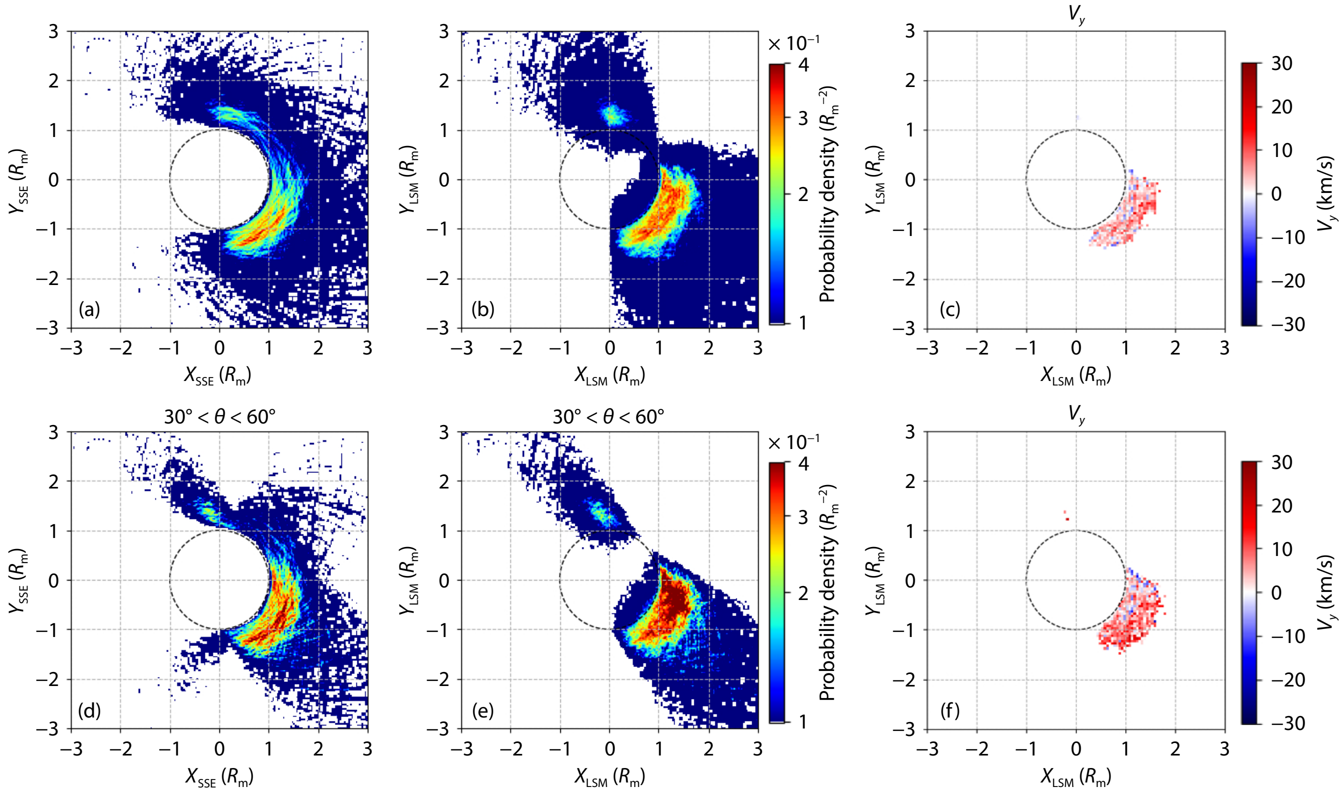

Figure 5. Probability density distributions of the positions (a,b,d,e) and V_y (c,f) of ARTEMIS probes when either probe P1 or P2 is magnetically connecting to the dayside of the Moon. (a) and (b) show the distribution in the SSE and LSM coordinate system; (c) shows the median value of V_y in each bin when the probability densities of the bins in panel (b) are larger than 0.2; (d) and (e) show the distribution in the SSE and LSM coordinate system when $30° < \theta < 60°$; θ represents the acute angle between the IMF and X axis; (f) shows the median value of V_y in each bin when the probability densities of the bins in Figure 5e are larger than 0.2. The number of the bins is 200 × 200. R_m represents the radius of the Moon.

simulation uses a fictitious size for the lunar body, which is only several times larger than the Debye length. Consequently, it still has difficulties in explaining the high-altitude perturbations of up to 1000 km shown in this paper. It seems that there is a component of solar wind electron with very high temperature and very low density (so that it has a very large Debye length) that is responsible for the large-scale potential drop around the Moon. If the velocity of this moonward deviation is related to the potential drop around the moon, then it also explains the larger velocity deviation at the regions further downstream, shown in Figure 5f. Due to the fact that the positive charge current caused by solar wind ions and photoelectrons decreases as the solar zenith angle decreases, we can obtain a reduced surface potential downstream, resulting in a larger velocity deviation.

The significant perturbations in the solar wind velocity observed upstream of the Moon at the IMFs connected to the dayside suggest a complex interaction mechanism. The systematic deviation of the solar wind flow in the $+Y$ direction (moonward) indicates that the magnetic field lines may play a crucial role in this process. When $30° < \theta < 60°$, the IMF lines pass through the Moon obliquely. This geometry allows for a more extended interaction time of the magnetic field lines with the lunar surface, which may enhance the deflection of the solar wind flow. The increasing deviation with increasing interaction times, as shown in Figure 5c and 5f, supports this hypothesis that this interaction may generate large-scale electric fields or magnetic structures that perturb the solar wind flow in a manner not yet fully understood. As the magnetic field lines are quasi-parallel to the solar wind velocity, although the field lines remain connected to the Moon for a quite long time, the flow deviation remains slight, indicating that the mechanism behind the flow perturbation does not tend to occur in this quasi-parallel condition.

The large-scale perturbations observed in the solar wind velocity upstream of the Moon's dayside, on the IMFs that are connected to the dayside of the Moon, cannot be fully explained by current understanding. Clearly, these perturbations cannot be attributed to the pickup of reflected ions or to the mechanisms that create flow disturbance in the lunar wake. The magnetic connectivity of the flow perturbations indicates that the Moon's solar wind interaction is crucial, but the specific mechanisms behind them remain unclear. This finding highlights the complexity of the solar wind interaction with the Moon. Further observational studies with higher spatial and temporal resolution could provide insights into the nature of the observed perturbations and help to uncover the underlying mechanisms.

5. Summary

This study reports unexpected large-scale moonward deviations of the solar wind velocities by the Moon, using 11 years of OMNI and ARTEMIS data spanning from January 1, 2012, to January 1, 2023. In the LSM coordinate system, systematic $+Y$ direction (moonward) solar wind flow deviations (~tens of km/s) occur when IMF lines connect to the dayside of the Moon, extending to altitudes of up to 1000 km (Figures 2b, 4c, 5c/f). The Parker spiral magnetic fields at the Moon are primarily in the ecliptic plane, pointing either toward or away from the Sun. The flow deviations are primarily observed upstream of the Moon along these Parker spiral magnetic fields. The oblique geometry of IMFs may generate a wider space ahead of the Moon that is magnetically connected to the lunar body, allowing for the greater interaction time of the incident solar wind with the magnetic field lines. This explains why we observed that, the longer the duration of the interaction, the greater the moonward deviation. The influence of the Moon's solar wind interactions on the formation of solar wind deviation is evident, but the exact underlying mechanisms remain unclear.

Acknowledgments

This work was supported by the National Natural Science Foundation of China (Grant No. 42474227, 42241106, 42388101). The authors thank the NASA/GSFC's Space Physics Data Facility for the OMNIWeb service at http://cdaweb.gsfc.nasa.gov/ for providing the data for the solar wind and the interplanetary magnetic fields. We also specially acknowledge with appreciation J. McFadden for use of ESA and K.H. Glassmeier, U. Auster, and W. Baumjohann for the use of FGM data provided under the lead of the Technical University of Braunschweig and with financial support through the German Ministry for Economy and Technology and the German Center for Aviation and Space (DLR) under contract 50 OC 0302. All ARTEMIS data necessary to reproduce this work are publicly available at http://artemis.ssl.berkeley.edu.

References

Angelopoulos, V. (2011). The ARTEMIS mission. *Space Sci. Rev.*, *165*(1-4), 3–25. https://doi.org/10.1007/s11214-010-9687-2

Auster, H. U., Glassmeier, K. H., Magnes, W., Aydogar, O., Baumjohann, W., Constantinescu, D., Fischer, D., Fornacon, K. H., Georgescu, E., … Wiedemann, M. (2008). The THEMIS fluxgate magnetometer. *Space Sci. Rev.*, *141*(1-4), 235–264. https://doi.org/10.1007/s11214-008-9365-9

Clack, D., Kasper, J. C., Lazarus, A. J., Steinberg, J. T., and Farrell, W. M. (2004). Wind observations of extreme ion temperature anisotropies in the lunar wake. *Geophys. Res. Lett.*, *31*(6), L06812. https://doi.org/10.1029/2003GL018298

Fatemi, S., Holmström, M., Futaana, Y., Lue, C., Collier, M. R., Barabash, S., and Stenberg, G. (2014). Effects of protons reflected by lunar crustal magnetic fields on the global lunar plasma environment. *J. Geophys. Res.: Space Phys.*, *119*(8), 6095–6105. https://doi.org/10.1002/2014ja019900

Freeman, J. W., and Ibrahim, M. (1975). Lunar electric fields, surface potential and associated plasma sheaths. *Moon*, *14*(1), 103–114. https://doi.org/10.1007/bf00562976

Halekas, J. S., Bale, S. D., Mitchell, D. L., and Lin, R. P. (2005a). Electrons and magnetic fields in the lunar plasma wake. *J. Geophys. Res.: Space Phys.*, *110*(A7), A07222. https://doi.org/10.1029/2004JA010991

Halekas, J. S., Delory, G. T., Farrell, W. M., Angelopoulos, V., McFadden, J. P., Bonnell, J. W., Fillingim, M. O., and Plaschke, F. (2011). First remote measurements of lunar surface charging from ARTEMIS: evidence for nonmonotonic sheath potentials above the dayside surface. *J. Geophys. Res.: Space Phys.*, *116*(A7), A07103. https://doi.org/10.1029/2011JA016542

Halekas, J. S., Lin, R. P., and Mitchell, D. L. (2005b). Large negative lunar surface potentials in sunlight and shadow. *Geophys. Res. Lett.*, *32*(9), L09102. https://doi.org/10.1029/2005GL022627

Lyon, E. F., Bridge, H. S., and Binsack, J. H. (1967). Explorer 35 plasma measurements in the vicinity of the Moon. *J. Geophys. Res.*, *72*(23), 6113–6117. https://doi.org/10.1029/JZ072i023p06113

McFadden, J. P., Carlson, C. W., Larson, D., Ludlam, M., Abiad, R., Elliott, B., Turin, P., Marckwordt, M., and Angelopoulos, V. (2008). The THEMIS ESA plasma instrument and in-flight Calibration. *Space Sci. Rev.*, *141*(1-4), 277–302. https://doi.org/10.1007/s11214-008-9440-2

Nakagawa, T., and Kimura, S. (2011). Role of the solar wind magnetic field in the interaction of a non-magnetized body with the solar wind: an electromagnetic 2-D particle-in-cell simulation. *Earth Planets Space*, *63*(6), 477–486. https://doi.org/10.5047/eps.2011.02.006

Ness, N. F., Behannon, K. W., Taylor, H. E., and Whang, Y. C. (1968). Perturbations of the interplanetary magnetic field by the lunar wake. *J. Geophys. Res.*, *73*(11), 3421–3440. https://doi.org/10.1029/JA073i011p03421

Ogilvie, K. W., and Ness, N. F. (1969). Dependence of the lunar wake on solar wind plasma characteristics. *J. Geophys. Res.: Space Phys.*, *74*(16), 4123–4128. https://doi.org/10.1029/JA074i016p04123

Poppe, A., Halekas, J. S., and Horányi, M. (2011). Negative potentials above the day-side lunar surface in the terrestrial plasma sheet: evidence of non-monotonic potentials. *Geophys. Res. Lett.*, *38*(2), L02103. https://doi.org/10.1029/2010gl046119

Sonett, C. P. (1982). Electromagnetic induction in the Moon. *Rev. Geophys.*, *20*(3), 411–455. https://doi.org/10.1029/RG020i003p00411

Whang, Y. C., and Ness, N. F. (1970). Observations and interpretation of the lunar mach cone. *J. Geophys. Res.*, *75*(31), 6002–6010. https://doi.org/10.1029/JA075i031p06002

Xu, S. S., Poppe, A. R., Halekas, J. S., and Harada, Y. (2020). Reflected protons in the lunar wake and their effects on wake potentials. *J. Geophys. Res.: Space Phys.*, *125*(7), e2020JA028154. https://doi.org/10.1029/2020ja028154

Zhang, H., Khurana, K. K., Kivelson, M. G., Angelopoulos, V., Wan, W. X., Liu, L. B., Zong, Q. G., Pu, Z. Y., Shi, Q. Q., and Liu, W. L. (2014). Three-dimensional lunar wake reconstructed from ARTEMIS data. *J. Geophys. Res.: Space Phys.*, *119*(7), 5220–5243. https://doi.org/10.1002/2014JA020111

Zhang, T. X., Zhang, H., Lai, H. R., Zhong, J., Liu, L. B., Wei, Y., Cao, J. B., Cui, J., Zhu, C. B., … Wan, W. X. (2020). Asymmetric lunar magnetic perturbations produced by reflected solar wind particles. *Astrophys. J. Lett.*, *893*(2), L36. https://doi.org/10.3847/2041-8213/ab8640